Published in final edited form as:
J Mol Biol. 2008 September 5; 381(3): 519–528. doi:10.1016/j.jmb.2008.06.029.

Similarities and Differences between Frozen-Hydrated, Rigor Acto-S1 Complexes of Insect Flight and Chicken Skeletal Muscles

Kimberly P. Littlefield[†],
The Scripps Research Institute, Dept. of Cell Biology, La Jolla, CA 92307

Andrew B. Ward,
The Scripps Research Institute, Dept. of Cell Biology, La Jolla, CA 92307

Joshua S. Chappie,
The Scripps Research Institute, Dept. of Cell Biology, La Jolla, CA 92307

Michael K. Reedy,
Duke University, Dept. of Cell Biology, Durham, NC 27710

Sanford I. Bernstein,
San Diego State University, Dept. of Biology and Molecular Biology Institute, San Diego, CA 92182-4614

Ronald A. Milligan, and
The Scripps Research Institute, Dept. of Cell Biology, La Jolla, CA 92307

Mary C. Reedy
Duke University, Dept. of Cell Biology, Durham, NC 27710

Summary

The structure and function of myosin crossbridges in asynchronous insect flight muscle (IFM) have been elucidated *in situ* using multiple approaches. These include generating “atomic” models of myosin in multiple contractile states by rebuilding the crystal structure of chicken sub-fragment 1 (S1) to fit IFM crossbridges in lower resolution EM tomograms and by “mapping” the functional effects of genetically-substituted, isoform-specific domains, including the converter domain, in chimeric IFM myosin to sequences in the crystal structure of chicken S1.

We prepared helical reconstructions (~25 Å resolution) to compare the structural characteristics of nucleotide-free myosin S1 bound to actin (acto-S1) isolated from chicken skeletal muscle (*CSk*), and the flight muscles of *Lethocerus* (*Leth*) wild-type *Drosophila (wt Dros)*, and a *Drosophila* chimeric myosin wherein the converter domain of the indirect flight muscle myosin isoform has been replaced by the embryonic skeletal myosin converter domain (*IFI-EC*). Superimposition of the maps of the frozen-hydrated acto-S1 complexes shows that differences between *CSk* and IFM S1 are limited to the azimuthal curvature of the lever arm: the regulatory light chain region of chicken skeletal S1 bends clockwise (as seen from the pointed end of actin) while those of IFM S1 project in a straight radial direction. All the IFM S1s are essentially identical other than some variation in the azimuthal spread of density in the regulatory light chain (RLC) region. This spread is most pronounced in the

Correspondence to: Kimberly P. Littlefield.
[†]Present Address: Center for Cell Dynamics, 620 University Rd., Friday Harbor, WA 98250

IFI-EC S1, consistent with proposals that the embryonic converter domain increases the compliance of the IFM lever arm affecting the function of the myosin motor. These are the first unconstrained models of IFM S1 bound to actin and the first direct comparison of the vertebrate and invertebrate skeletal myosin II classes, the latter for which data on the structure of discrete acto-S1 complexes are not readily available.

Keywords

myosin; actin; *Drosophila*; *Lethocerus*; converter domain

Three dimensional (3D) visualization and modeling of myosin crossbridges, in relaxed, contracting, and rigor states *in-situ*, has been extensively pursued in the well ordered asynchronous insect flight muscle (IFM) of the giant waterbug *Lethocerus indicus* (*Leth*). Electron tomograms of fast frozen, freeze-substituted IFM reveal the 3D envelope of the myosin head (when bound to actin) in detail. The internal molecular machinery, however, has been modeled by crystal structures of myosin heads (myosin sub-fragment 1 (S1)) or other smaller expressed fragments of numerous myosin isoforms from other species [1; 2; 3] (for reviews see [4; 5]).

Leth are collected in the wild as they cannot be raised or maintained in the lab. As a result, the numbers of insects needed for large-scale crystallographic studies of *Leth* myosin are not available. Dissection of thousands of 1 mm flight muscles from *Drosophila melanogaster* (*wt Dros*) - the fruit-fly, for X-ray crystallography is also not practical. This leaves open the questions of whether IFM and vertebrate skeletal myosin S1 differ in head structure when bound to actin and when free from the constraints imposed by the whole myosin molecule and the filament lattice.

Cryo electron microscopy (cryo-EM) provides sufficient resolution to detect subtle changes in S1 heads bound to actin in native conformations [6; 7], free of their linkage to a partner head and the constraints of the *in situ* lattice. To study the structure of the acto-myosin complex of insects and to compare it to vertebrates, we prepared helical reconstructions (~25 Å) of nucleotide-free myosin S1 bound to actin (acto-S1) from chicken skeletal muscle (*CSk*), indirect flight muscles of *Leth*, *wt Dros*, and a *Drosophila* chimeric myosin, *IFI-EC* [15], wherein the converter domain of the indirect flight isoform has been replaced by the embryonic skeletal myosin converter domain.

Molecular morphology of vertebrate and invertebrate acto-S1 complexes is the same

Fig. 1 shows surface views of density maps obtained by cryo-EM of frozen-hydrated S1 preparations purified from *CSk* (A), *wt Dros* (B), *IFI-EC* (C), and *Leth* (D) bound to rabbit skeletal actin in rigor. All these acto-S1 complexes show the characteristic [8] arrowhead appearance of F-actin saturated with rigor S1 heads bound to the actin surface and the long (85Å) light chain binding domain projecting out from the filament. Discrete features of individual S1 heads, including the motor domain (MD), and essential (ELC) and regulatory (RLC) light binding regions are visible in all preparations. The RLC domain of frozen-hydrated S1 exhibits some disorder [6; 8; 9] due to Brownian motion and the loss of some RLC during S1 isolation. Moreover, in both the *IFI-EC* and *Leth* maps we observe a prominent azimuthal spread of density in the RLC region, which we have dubbed the "whale tail."

Comparison of the insect acto-S1 complexes: wt Dros and Leth maps are identical

We compared the two different wild-type insect acto-S1 preparations by superimposing helical 3D reconstructions in wireframe, stereo view at ~25 Å resolution. As shown in Fig. 2A, acto-S1s derived from *wt Dros* (red) and *Leth* (cyan) IFM, are essentially identical through the motor domain and essential light chain regions. Differences between the two preparations are limited to the RLC region, where, in the *Leth* map we observe more positional variation of the RLC region (noise). These data suggest that the *Leth* S1 head may have evolved greater flexibility in the LCD and/or RLC regions relative to *wt Dros*.

Comparison of the wt Dros and IFI-EC acto-S1 complexes: substitution of the embryonic converter domain alters the compliance of the RLC region

Because of its genetic tractability, *wt Dros* presents a compelling opportunity to define whether or how discrete domains within the myosin head differ in structure. To date direct comparisons of unstrained conformations of *wt Dros* IFM S1 and any type of chimeric IFM S1 bound to actin have not been reported.

Tissue-specific *wt Dros* skeletal myosin isoforms are generated by alternative splicing of 6 sets of exons within the single myosin heavy chain (MHC) gene [10]. MHC isoform expression profiles and protein sequences are known in *Dros* ([11; 12] for review see [13]). While the converter domain (encoded by exon 11e) is expressed only in IFM myosin, the other *wt Dros* MHC converter sequences (encoded by isovarients exon 11 a–d) are used in the other fourteen *wt Dros* MHC isoforms. Exon 11 encodes the proximal end of the converter domain (residues corresponding to amino acids 724–764 in the chicken skeletal muscle sequence) that likely interacts with the distal end of the relay helix (encoded by alternatively spliced exon 9) and/or the N-terminus of the protein (encoded by alternatively spliced exon 3). MHC chimeras, like the IFI-EC wherein the slow, embryonic body wall muscle myosin converter domain is substituted into the IFM myosin and expressed in the IFM of transgenic flies, show altered function, both *in-situ* and *in-vitro*. Functional differences in chimeric molecules are attributable solely to these domain substitutions [14; 15; 16; 17; 18; 19; 20; 21].

The converter domain is thought to translate (convert) and amplify events in the nucleotide-binding site associated with ATP hydrolysis to the light-chain binding domain (LCD) or “lever arm”. ATPase values are dramatically elevated in the IFI-EC isoform but actin filament velocities and tension redevelopment (r^3) are slower [15; 18]. This apparent contradiction between the solution biochemistry and both the unloaded (in-vitro motility velocities) and loaded (fiber mechanics data) functional properties of the IFI-EC chimera has been proposed to reflect effects of the converter on the kinetics of lever arm movement, through increased compliance of the lever arm. This implies that structural differences conferred by substitution of the embryonic converter into the IFM myosin could be dramatic.

As shown in Fig. 2B, the disorder around the RLC, or "whale tail," is especially pronounced in the *IFI-EC* chimera (pink wireframe), when compared to the *wt Dros* (red wireframe). These data suggest that there is a significant increase in the compliance of the RLC region when the embryonic converter is substituted into the *wt Dros* IFM isoform.

The structure of the *IFI-EC* motor domain, is at this resolution however, identical to that of the other isoforms. When all of the insect maps are truncated after the ELC, excluding the “noisy” RLC density, the structural similarity of all the maps is emphasized (Fig. 2C).

Comparison of the chicken skeletal and insect acto-S1 complexes: the azimuthal slew and bend of the RLC regions differs between the CSk and IFM acto-S1 preparations

When the *CSk* (blue, surface view) and *wt Dros* (red, wireframe) acto-S1 maps are superimposed (Fig. 3A) there is a prominent region of non-overlap in the RLC region. In a similar representation (Fig. 3B), the CSk acto-S1 map (blue, surface view) superimposed with *Leth* acto-S1 map (cyan, wireframe) also shows the same extent of non-overlap of the RLC region even when the wide spread of noisy "whale tail" density in the RLC region is included.

The differences between the vertebrate and insect acto-S1 complexes are reinforced by viewing the *CSk* acto-S1 wireframe map (blue) superimposed with the *wt Dros* (red), *Leth* (cyan), IFI-EC (white) wireframe maps truncated just after the ELC region. In longitudinal view (Fig. 3C), divergence of the chicken and IFM lever arms beginning in the ELC region is observed in all of the insect maps (*wt Dros* (red), *Leth* (cyan), and *IFI-EC* (white)) relative to CSk (blue). The LCD of chicken S1 is more azimuthally slewed and bent than any of the IFM S1s, which project in a straight radial direction away from the ELC region even when the noisy RLC data are not included.

Atomic modeling of vertebrate and insect acto-S1 EM densities with the chicken S1 crystal structure

To better define crossbridge structure, modeling has been performed in EM tomograms using the nucleotide-free chicken myosin S1 crystal structure docked on vertebrate actin [22; 23]. Fitting the vertebrate S1 crystal structure into rigor IFM crossbridge envelopes requires significant bending of the LCD - lever arm- especially in the azimuthal direction [3; 24]. Fig. 4 shows that even when the chicken crystal acto-S1 is docked on the actin filament [23] within the chicken acto-S1 complex (Fig. 4A - stereo, longitudinal view), the crystal structure does not exactly match the LCD density of even the *CSk* acto-S1 map, consistent with other reports [25]. When the maps (*CSk*, *wt Dros*, *IFI-EC*, and *Leth*) and the atomic model are superimposed and viewed in cross section (Fig. 4B) or longitudinally (Fig. 4C) the atomic model of the LCD appears midway between the RLC regions of the *CSk* and IFM maps.

These results are consistent with other data [26] that showed differences between crystallized S1 and S1 bound to actin *in-vitro* using negative stain and single particle analysis. We observe that when the chicken S1 crystal structure [22] is docked into the acto-S1 density, the angle of the LCD especially, is not well accommodated in either the chicken or insect acto-S1 EM density maps. Iterative fitting procedures that have quantitatively modeled the atomic S1 structure into frozen-hydrated acto - skeletal and smooth S1 complexes result in similar accommodation problems [27]. The S1 atomic model [22] was extensively rebuilt [2] to fit the full range of crossbridge powerstroke positions identified in the intact fibrillar lattice of *Leth*. Manual rebuilding of the atomic model of the chicken S1 required axial and azimuthal adjustments of the LCD of the crystal structure to fit into the envelopes of crossbridges under strain and some prestroke heads also required movement of the motor domain. If used to model crossbridges in tomograms of *Leth* IFM the straighter radial profile and the lesser bend and slew of the unconstrained IFM S1 that we observe would require less azimuthal bending to match bridge envelopes, but significant movements of nucleotide-free S1 would still be required to fit active IFM crossbridges.

How does the compliance of the LCD relate to the functional properties of the insect flight muscle myosin?

Direct comparison of these helical reconstructions of frozen-hydrated *CSk* and IFM acto-S1 helps define the unconstrained conformations of nucleotide-free myosin heads bound to actin. At this intermediate resolution, differences between the acto-S1 complexes appear limited to the RLC region of the LCD “lever arm”. The vertebrate S1 is slightly more axially angled and clearly more azimuthally slewed than the insect IFM S1. If, as previously described [28], the LCD is a marker of the position of the converter domain, the structural coupling between the motor domain and LCD through the converter domain in the insect preparations appears to be adapted for the constraints of the stiff lattice necessary to achieve the high wing beat frequencies that support flight.

In both the *Leth* and *IFI-EC* chimera maps we observe a considerable azimuthal spread of density in the RLC-region as compared to both *wt Dros* and *CSk*. This "whale tail” of density in the RLC region of the lever arm is consistent with increased compliance around a pivot point in the LCD that allows the RLC region to adopt multiple positions. The converter domain is thought to link hydrolytic events in the ATP pocket to movement of the LCD or lever arm (for review see [29]). In the *IFI-EC* chimera, increased compliance in the linkage between nucleotide hydrolysis, converter, and lever arm could explain both the increased ATPase rates in solution and the reduced *in-vitro* motility velocities [15; 18]. If the converter slips out-of- “gear,” hydrolysis rates could soar while actin filament velocity would decrease, rather like racing an engine with the transmission (converter) in neutral. However, the IFI-EC myosin can support flight [15], suggesting that some mechanism is compensating for any extra compliance in the RLC region, possibly the high stiffness of the IFM filament lattice and adjustment of the wing beat frequency.

Chicken skeletal muscle and insect IFM preparations show similar S1 structures but have widely divergent filament and crossbridge lattices

The slight differences in the azimuthal positions of the vertebrate and insect LCD regions do not discount the fact that the vertebrate and insect preparations have - essentially, identical S1 structures. It is significant that similar S1 structures have adapted to widely divergent filament and crossbridge lattices and broadly varying functional demands (for reviews see [5; 30; 31]). For example, in vertebrates (chicken), actin filaments are at trigonal positions where they receive myosin crossbridges from three thick filaments. However, in all stretch-activated, asynchronous IFM filament lattices, actin filaments are located at dyad positions and receive crossbridges from two flanking thick filaments. This structural arrangement affects the frequency with which myosin heads find target actins. Moreover, vertebrate thick filaments are 1.6 microns long, where as IFM thick filaments are 2.8–3.0 microns long and are also much stiffer; affecting power output. IFM operates at nearly full filament overlap (5% maximum length change), in contrast to the wider sarcomere length variation in vertebrates. Wt *Dros* IFM differs from *Leth* in having a superlattice in which adjacent thick filaments are axially staggered [32] and a relaxed myosin head arrangement less ordered than *Leth*. Yet, both IFM generate more power, at higher oscillatory frequencies, than chicken skeletal muscle. In contrast, super-contractile, slow, embryonic body wall myosin in the insect differs from both IFM and *CSk* in all these parameters. For example, body-wall muscle is characterized by perforated Z-discs and a lattice wherein each long, thick filament is surrounded by an irregular arrangement of 8–12 actin filaments [33].

The compliance of the myosin lever arm modulates force and motion generation [34] and is an important determinant of the fidelity with which crossbridges bind to actin targets at varying

filament spacings. The most extreme example of an unusual actin presentation is the formation of reverse rigor crossbridge attachments to oppositely polarized actin in the flightless *Dros* IFM actin mutant G6A,A7T that requires the myosin heads to twist ~180° around the S2 [35]. Another example of "adaptation of actin acess due to differences in filament spacing and arrangement is observed between *wt Dros* IFM and embryonic body wall muscles. The filament stagger in the superlattice of *wt Dros* IFM confines and facilitates rapid myosin attachment/detachment to actin target zones over a relatively short distance. The very large sarcomere length variation and less regular thin filament positions in supercontractile embryonic muscles requires myosin heads to find actin binding sites through relatively slow collisional encounters and then to exert force over a range of filament spacings. Therefore, variation in the flexibility and compliance of the S1 lever arm (particularly in the RLC region) would be advantageous. Small differences in S1 structure, such as what we observe here, suggest alterations in the compliance of the lever arm may be sufficient to adapt very similar S1 structures to differing environments.

Acknowledgements

We thank Mr. Corey Dambacher and Ms. Jennifer Suggs for *wt Dros* and *IFI-EC* dissection assistance and Drs. Ryan Littlefield and Douglas Swank for critical reading of this manuscript. K. P. Littlefield was supported by American Heart Association Western States Affiliate postdoctoral fellowship 0120127Y and NIH 5P50 GM066050, S.I. Bernstein by NIH NCRR P41 RR-17573, GM-32443, M.K. Reedy by R37 AR-14317, and R.A. Milligan by AR-39155. Funding for the development of UCSF Chimera comes from an NIH NCRR grant P41 RR-01081.

Bibliography

1. Squire JM, Al-Khayat HA, Harford JJ, Hudson L, Irving T, Knupp C, Reedy MK. Modelling muscle motor conformations using low-angle X-ray diffraction. IEE Proc Nanobiotechnol 2003;150:103–110. [PubMed: 16468939]
2. Taylor KA, Schmitz H, Reedy MC, Goldman YE, Franzini-Armstrong C, Sasaki H, Tregear RT, Poole K, Lucaveche C, Edwards RJ, Chen LF, Winkler H, Reedy MK. Tomographic 3D reconstruction of quick-frozen, Ca2+-activated contracting insect flight muscle. Cell 1999;99:421–431. [PubMed: 10571184]
3. Liu J, Reedy MC, Goldman YE, Franzini-Armstrong C, Sasaki H, Tregear RT, Lucaveche C, Winkler H, Baumann BA, Squire JM, Irving TC, Reedy MK, Taylor KA. Electron tomography of fast frozen, stretched rigor fibers reveals elastic distortions in the myosin crossbridges. J Struct Biol 2004;147:268–282. [PubMed: 15450296]
4. Reedy MC. Visualizing myosin's power stroke in muscle contraction. J Cell Sci 2000;113(Pt 20):3551–3562. [PubMed: 11017871]
5. Squire JM, Knupp C, Roessle M, Al-Khayat HA, Irving TC, Eakins F, Mok NS, Harford JJ, Reedy MK. X-ray diffraction studies of striated muscles. Adv Exp Med Biol 2005;565:45–60. [PubMed: 16106966]discussion 359–69.
6. Whittaker M, Wilson-Kubalek EM, Smith JE, Faust L, Milligan RA, Sweeney HL. A 35-Å movement of smooth muscle myosin on ADP release. Nature 1995;378:748–751. [PubMed: 7501026]
7. Volkmann N, Hanein D, Ouyang G, Trybus KM, DeRosier DJ, Lowey S. Evidence for cleft closure in actomyosin upon ADP release. Nat Struct Biol 2000;7:1147–1155. [PubMed: 11101898]
8. Milligan RA, Flicker PF. Structural relationships of actin, myosin, and tropomyosin revealed by cryo-electron microscopy. J Cell Biol 1987;105:29–39. [PubMed: 3611188]
9. Jontes JD, Wilson-Kubalek EM, Milligan RA. A 32 degree tail swing in brush border myosin I on ADP release. Nature 1995;378:751–753. [PubMed: 7501027]
10. George EL, Ober MB, Emerson CP Jr. Functional domains of the Drosophila melanogaster muscle myosin heavy-chain gene are encoded by alternatively spliced exons. Mol Cell Biol 1989;9:2957–2974. [PubMed: 2506434]
11. Hastings GA, Emerson CP Jr. Myosin functional domains encoded by alternative exons are expressed in specific thoracic muscles of Drosophila. J Cell Biol 1991;114:263–276. [PubMed: 2071673]

12. Zhang S, Bernstein SI. Spatially and temporally regulated expression of myosin heavy chain alternative exons during Drosophila embryogenesis. Mech Dev 2001;101:35–45. [PubMed: 11231057]

13. Bernstein SI, Milligan RA. Fine tuning a molecular motor: the location of alternative domains in the Drosophila myosin head. J Mol Biol 1997;271:1–6. [PubMed: 9300050]

14. Swank DM, Wells L, Kronert WA, Morrill GE, Bernstein SI. Determining structure/function relationships for sarcomeric myosin heavy chain by genetic and transgenic manipulation of Drosophila. Microsc Res Tech 2000;50:430–442. [PubMed: 10998634]

15. Swank DM, Knowles AF, Suggs JA, Sarsoza F, Lee A, Maughan DW, Bernstein SI. The myosin converter domain modulates muscle performance. Nat Cell Biol 2002;4:312–316. [PubMed: 11901423]

16. Swank DM, Bartoo ML, Knowles AF, Iliffe C, Bernstein SI, Molloy JE, Sparrow JC. Alternative exon-encoded regions of Drosophila myosin heavy chain modulate ATPase rates and actin sliding velocity. J Biol Chem 2001;276:15117–15124. [PubMed: 11134017]

17. Swank DM, Braddock J, Brown W, Lesage H, Bernstein SI, Maughan DW. An alternative domain near the ATP binding pocket of Drosophila myosin affects muscle fiber kinetics. Biophys J 2006;90:2427–2435. [PubMed: 16399836]

18. Littlefield KP, Swank DM, Sanchez BM, Knowles AF, Warshaw DM, Bernstein SI. The converter domain modulates kinetic properties of Drosophila myosin. Am J Physiol Cell Physiol 2003;284:C1031–C1038. [PubMed: 12477668]

19. Miller BM, Nyitrai M, Bernstein SI, Geeves MA. Kinetic analysis of Drosophila muscle myosin isoforms suggests a novel mode of mechanochemical coupling. J Biol Chem 2003;278:50293–50300. [PubMed: 14506231]

20. Miller BM, Zhang S, Suggs JA, Swank DM, Littlefield KP, Knowles AF, Bernstein SI. An alternative domain near the nucleotide-binding site of Drosophila muscle myosin affects ATPase kinetics. J Mol Biol 2005;353:14–25. [PubMed: 16154586]

21. Miller BM, Bloemink MJ, Nyitrai M, Bernstein SI, Geeves MA. A variable domain near the ATP-binding site in Drosophila muscle myosin is part of the communication pathway between the nucleotide and actin-binding sites. J Mol Biol 2007;368:1051–1066. [PubMed: 17379245]

22. Rayment I, Rypniewski WR, Schmidt-Base K, Smith R, Tomchick DR, Benning MM, Winkelmann DA, Wesenberg G, Holden HM. Three-dimensional structure of myosin subfragment-1: a molecular motor. Science 1993;261:50–58. [PubMed: 8316857]

23. Lorenz M, Popp D, Holmes KC. Refinement of the F-actin model against X-ray fiber diffraction data by the use of a directed mutation algorithm. J Mol Biol 1993;234:826–836. [PubMed: 8254675]

24. Liu J, Wu S, Reedy MC, Winkler H, Lucaveche C, Cheng Y, Reedy MK, Taylor KA. Electron tomography of swollen rigor fibers of insect flight muscle reveals a short and variably angled S2 domain. J Mol Biol 2006;362:844–860. [PubMed: 16949613]

25. Volkmann N, Ouyang G, Trybus KM, DeRosier DJ, Lowey S, Hanein D. Myosin isoforms show unique conformations in the actin-bound state. Proc Natl Acad Sci U S A 2003;100:3227–3232. [PubMed: 12612343]

26. Burgess SA, Walker ML, White HD, Trinick J. Flexibility within myosin heads revealed by negative stain and single-particle analysis. J Cell Biol 1997;139:675–681. [PubMed: 9348284]

27. Holmes KC, Schröder RR, Sweeney HL, Houdusse A. The structure of the rigor complex and its implications for the power stroke. Philos Trans R Soc Lond B Biol Sci 2004;359:1819–1828. [PubMed: 15647158]

28. Burgess S, Walker M, Wang F, Sellers JR, White HD, Knight PJ, Trinick J. The prepower stroke conformation of myosin V. J Cell Biol 2002;159:983–991. [PubMed: 12499355]

29. Geeves MA, Holmes KC. Structural mechanism of muscle contraction. Annu Rev Biochem 1999;68:687–728. [PubMed: 10872464]

30. Craig R, Woodhead JL. Structure and function of myosin filaments. Curr Opin Struct Biol 2006;16:204–212. [PubMed: 16563742]

31. Tregear RT, Reedy MC, Goldman YE, Taylor KA, Winkler H, Franzini-Armstrong C, Sasaki H, Lucaveche C, Reedy MK. Cross-bridge number, position, and angle in target zones of cryofixed isometrically active insect flight muscle. Biophys J 2004;86:3009–3019. [PubMed: 15111415]

32. Squire JM, Bekyarova T, Farman G, Gore D, Rajkumar G, Knupp C, Lucaveche C, Reedy MC, Reedy MK, Irving TC. The myosin filament superlattice in the flight muscles of flies: A-band lattice optimisation for stretch-activation? J Mol Biol 2006;361:823–838. [PubMed: 16887144]

33. Cripps RM, Suggs JA, Bernstein SI. Assembly of thick filaments and myofibrils occurs in the absence of the myosin head. Embo J 1999;18:1793–1804. [PubMed: 10202143]

34. Warshaw DM, Guilford WH, Freyzon Y, Krementsova E, Palmiter KA, Tyska MJ, Baker JE, Trybus KM. The light chain binding domain of expressed smooth muscle heavy meromyosin acts as a mechanical lever. J Biol Chem 2000;275:37167–37172. [PubMed: 10945998]

35. Reedy MC, Beall C, Fryberg CC. Formation of reverse rigor chevrons by myosin heads. Nature 1989;339:481–483. [PubMed: 2725681]

36. Margossian SS, Lowey S. Preparation of myosin and its subfragments from rabbit skeletal muscle. Methods Enzymol 1982;85(Pt B):55–71. [PubMed: 6214692]

37. Pardee JD, Spudich JA. Purification of muscle actin. Methods Enzymol 1982;85(Pt B):164–181. [PubMed: 7121269]

38. Margossian SS, White HD, Lefford J, Holt JC, Malhotra A, Stafford WF, Slatter HS. Functional effects of LC1-reassociation with cardiac papain Mg S1. J Mus Res Cell Mot 1993;14:3–14.

39. Weeds AG, Pope B. Studies on the chymotryptic digestion of myosin. Effects of divalent cations on proteolytic susceptibility. J Mol Biol 1977;111:129–157. [PubMed: 323500]

40. Carragher B, Whittaker M, Milligan RA. Helical processing using PHOELIX. J Struct Biol 1996;116:107–112. [PubMed: 8742731]

41. Jones TAZ, Cowan S, Kjeldgaard M. Improved methods for building models in electron density maps and the location of errors in these models. Acta. Crystallogr., Section A 1991:110–119. [PubMed: 2025413]

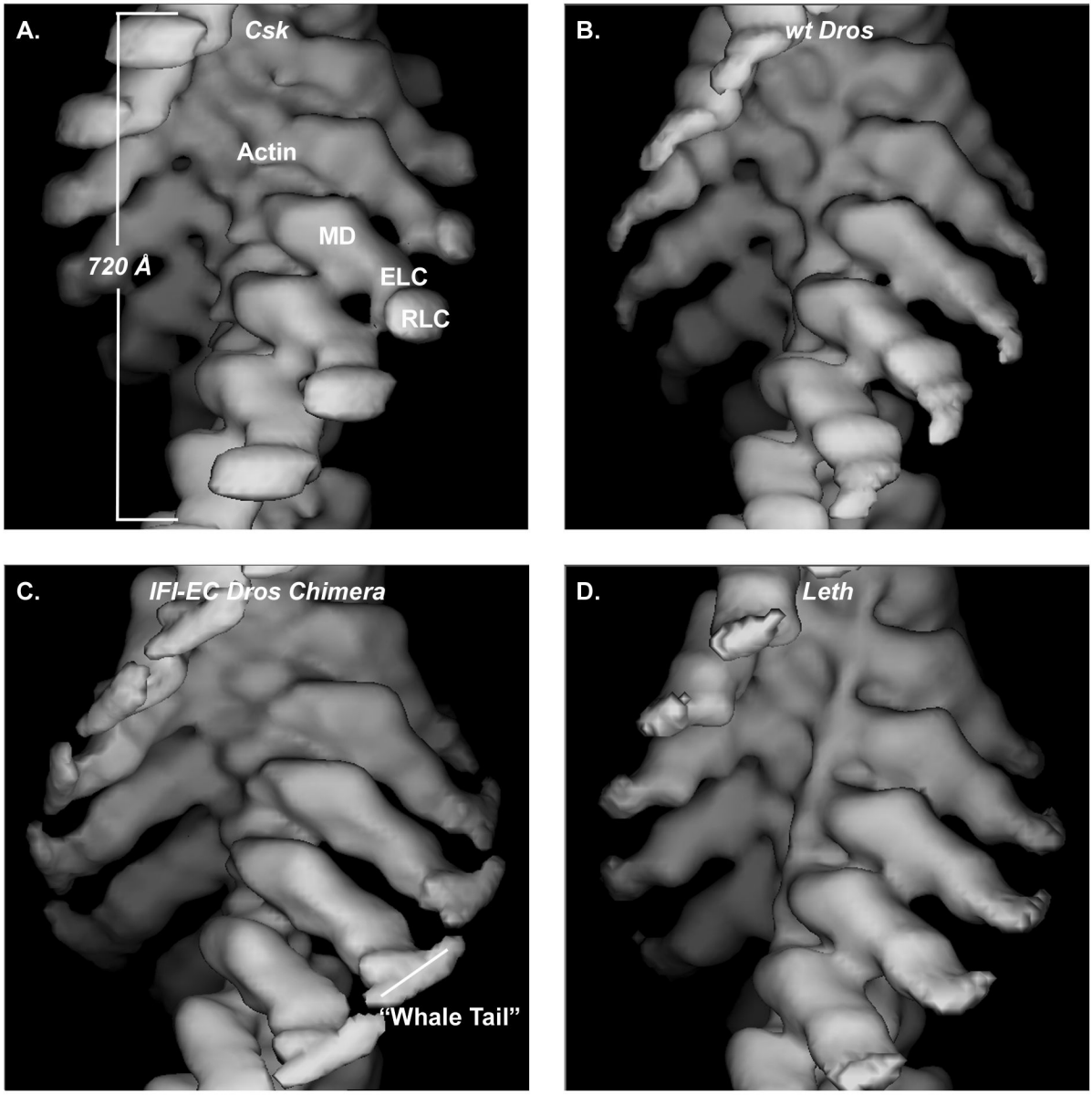

Figure 1.

Surface views of one 360° helical repeat (~720Å) of rigor acto-*CSk* S1 **(A)** acto-*wt Dros* S1 **(B)**, acto-*IFI-EC* S1 **(C)**, and acto-*Leth* **(D)** density maps. The acto-S1 complexes share similar features including identical actin-motor domain positions and a long (~85 Å) LCD projecting away from the actin filament, labeled in panel A: MD - motor domain, ELC- essential light chain region, RLC-regulatory light chain region. ***Protein Purification***. Skeletal myosin was prepared from chicken pectoralis muscle as previously described [36]. Myosin from insect IFM was purified from either half of a single *Leth* thorax or ~ 300 *wt Dros* or 450–500 IFI-EC thoraces (per myosin preparation) as previously described [18]. The *wt Dros* myosin yield was ~ 3.5 μg/fly where as the routine myosin yield from one *Leth* half thorax was ~ 500 μg. F-actin was prepared from rabbit muscle as previously described [37]. ***S1 Preparation***. The papain-Mg^{2+} myosin chicken S1 fragment was prepared as previously described [38] with the following modifications. Briefly, myosin at 5 – 20 mg/ml was suspended in 0.2 M ammonium acetate (pH 7.0), 2 mM $MgCl_2$, and 1 mM DTT. The protein was digested with 0.03 mg papain

(Worthington Biochemicals, Lakewood, NJ-activated at 1 mg/ml as per manufacturers instructions) per ml of myosin solution for 8 min. at 25°C. The reaction was stopped with 3 mM iodoacetic acid with one mini protease inhibitor tablet added/10ml solution (Roche Biochem, Mannheim, Germany) and placed on ice. The suspension was subjected to ultra-centrifugation (218 K × *g*) for 30 min. at 4°C to pellet the undigested myosin and rod while the soluble S1 fragment remained in solution. Insect S1 was prepared in a similar manner with the following exceptions: whole myosin was resuspended at 2 – 4 mg/ml in 2 mM KCl, 3 mM EDTA, pH 7.0, 20 mM potassium phosphate, pH 6.7, 5 mM β-mercaptoethanol and 5 mM $MgCl_2$ and digested with papain at 1:1000 w/w, enzyme to total protein, activated as described above, for 14–17 min. at 25°C. Longer digestion times yielded more S1 but resulted in significant digestion of the regulatory light chain. Concentration was determined using the $E^{1\%}_{280}$ = 7.5, molecular weight of ~90 KD [39]. S1 purity was assessed by SDS-PAGE. ***Acto-S1 complex preparation***. Rabbit F-actin (0.05 mg/ml) was decorated with rigor (nucleotide free) S1 on holey copper carbon-coated grids (400 mesh, Ted Pella, Inc., Redding, CA, or 400 mesh Quantifoil, Structure Probe, Inc., West Chester, PA). Specimens were frozen in liquid ethane and stored in liquid nitrogen. ***Cryo-electron microscopy and image analysis.*** Specimens were examined with a Philips CM200 FEG (120 kV, 36K × magnification, −178°C). Images were acquired at 1.5–1.8 .m under focus using low dose conditions on Kodak SO-163 film. Fully decorated filaments were scanned (Perkin Elmer 1010 scanner) and subjected to helical image analysis using Phoelix [40]. See Table 1 for a summary of the data and image processing results. S1 modeling was done manually using the program O [41] and the figures were created with AVS (Advanced Visual Systems, Inc., Waltham, MA).

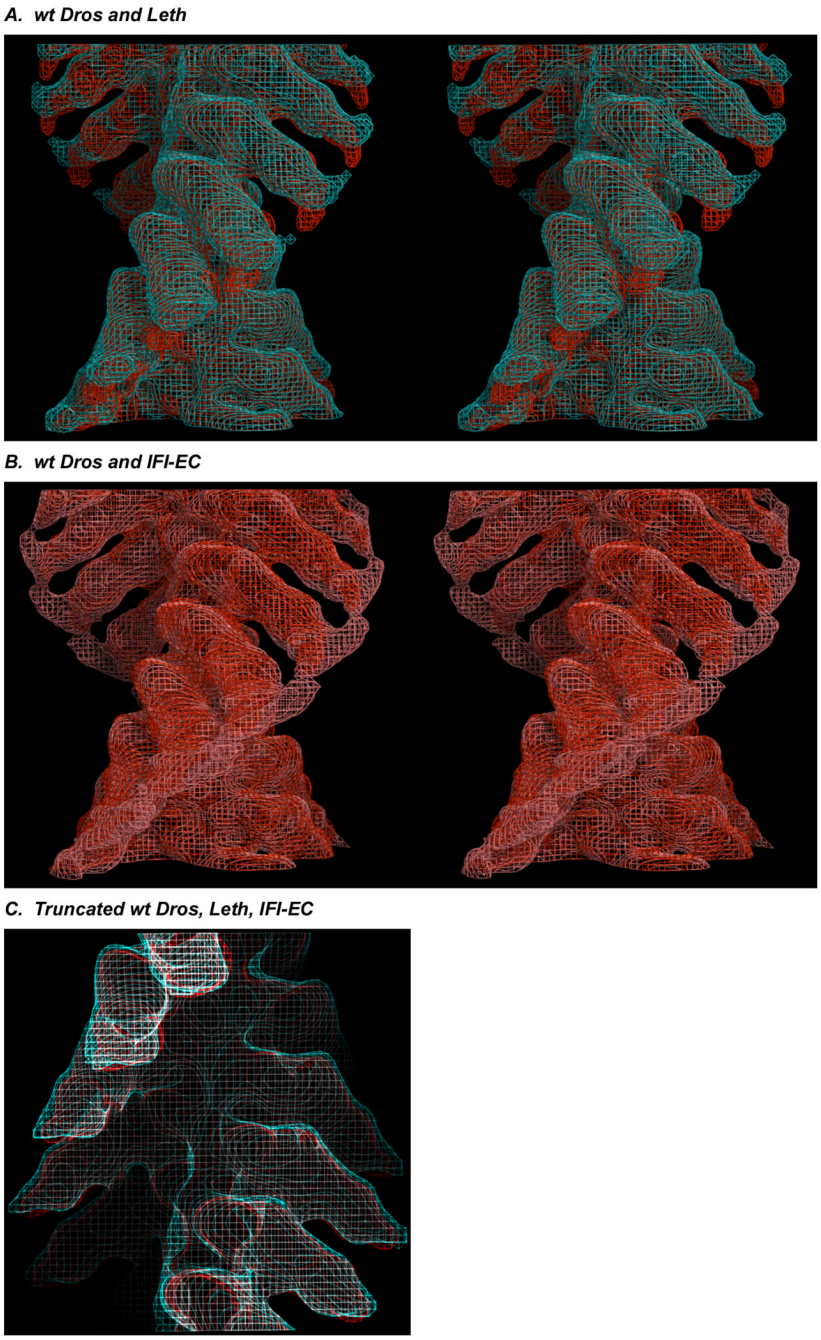

Figure 2.

(A) Stereo, longitudinal view of the *wt Dros* (red) and *Leth* (cyan) insect acto-S1 maps superimposed in wire frame. Stereo images were prepared used MacPyMol (DeLano Scientific). Density is identical in the insect maps through the motor domain and the ELC region of the LCD. **(B)** Comparison of the *wt Dros* (red) and *IFI-EC* chimera (pink) maps. When viewed longitudinally, in stereo, a prominent spread of density in the RLC region of the IFI-EC chimera map is apparent. This very noisy "whale tail" suggests the RLC region of chimeric S1 adopts multiple positions. **(C)**. Longitudinal view of the all of the insect maps. The similarity of the insect maps is emphasized by truncating the maps after the ELC omitting the "noisy" RLC region. *wt Dros*, red, *Leth*, cyan, *IFI-EC*, white.

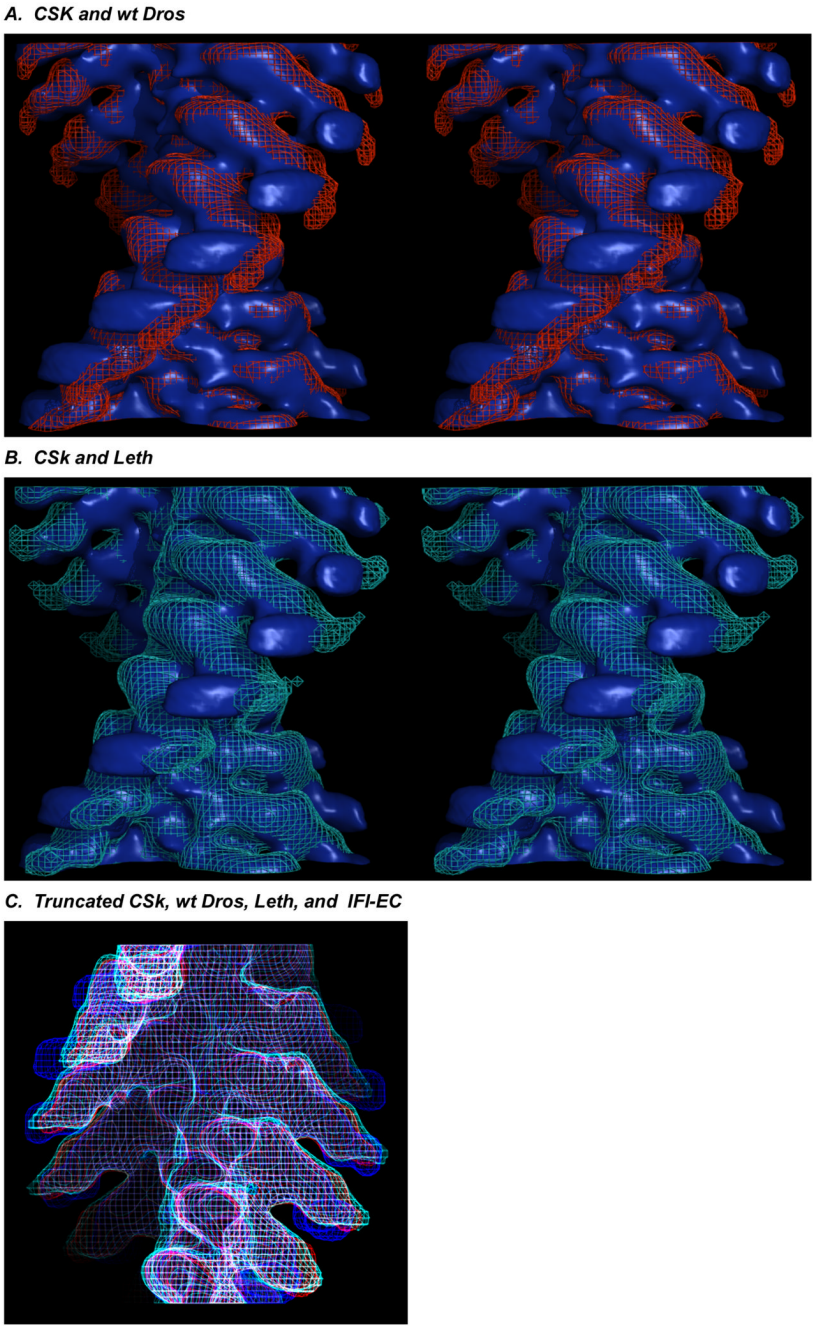

Figure 3.

Stereo, longitudinal view of acto-*CSk* S1 map (blue surface) superimposed with **(A)** *wt Dros* wireframe (red) and **(B)** *Leth* wireframe (cyan) maps shows the non-overlap regions. Stereo images were prepared used MacPyMol (DeLano Scientific). **(C)** *CSk* (blue wireframe) superimposed with *wt Dros* (red), *IFI-EC* (white) and *Leth* (cyan) maps truncated after the ELC.

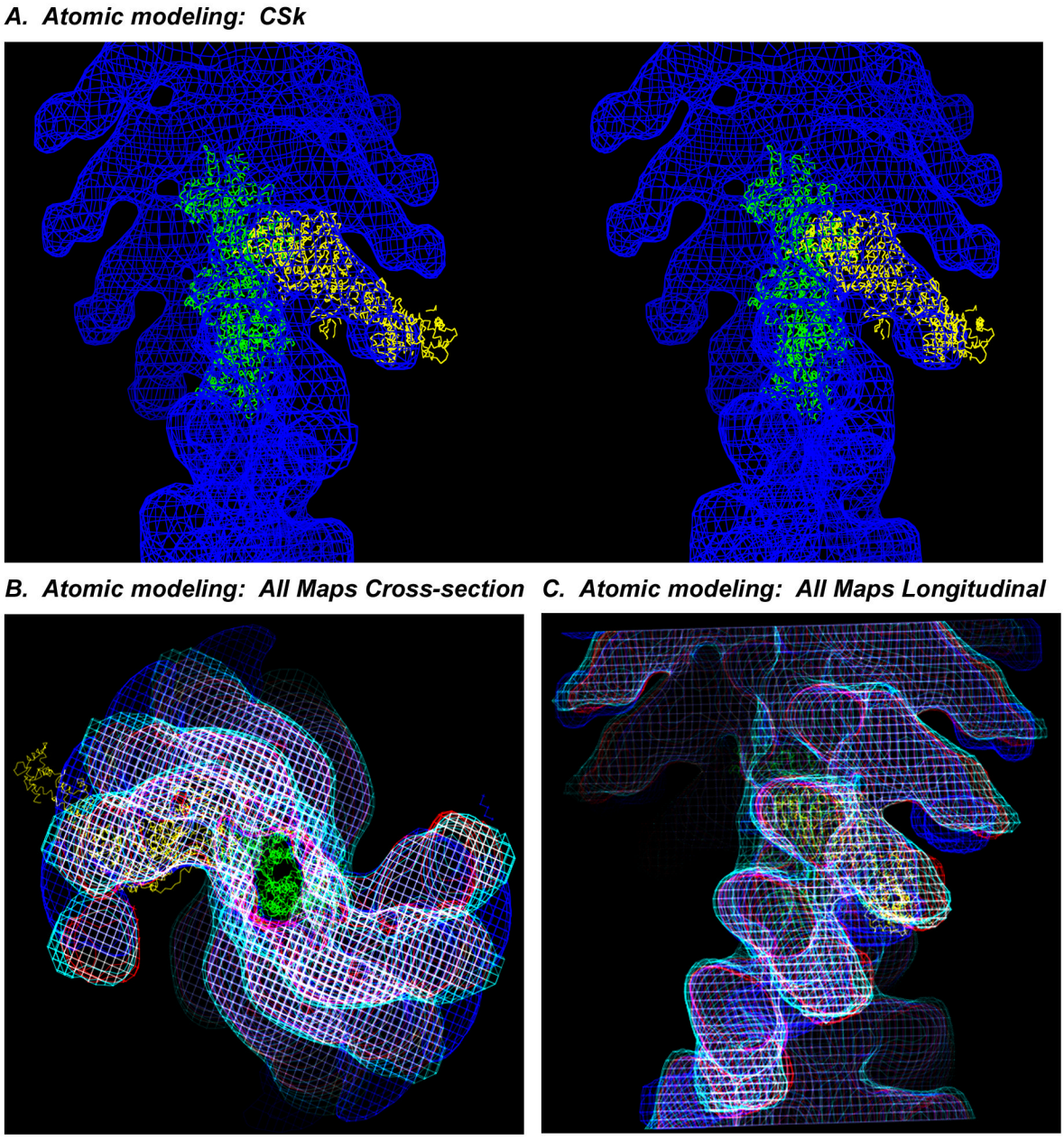

Figure 4.

(A) Nucleotide-free, chicken skeletal S1 crystal structure [22] (yellow) docked on actin [23] (green) modeled into the acto-*CSk* S1 map (blue, wireframe) in stereo, longitudinal view. Stereo image was prepared using the UCSF Chimera package from the Resource for Biocomputing, Visualization, and Informatics at the University of California, San Francisco. The RLC region of the crystal structure protrudes from the S1 envelope. **(B)** Cross-section and **(C)** longitudinal views of all of the density maps in wire frame superimposed, *CSk* (blue), *wt Dros* (red), *Leth* (cyan), *IFI-EC* (white), and compared to the nucleotide-free, chicken crystal structure (yellow) docked on actin (green) in the actoS1 reconstructions. Truncation of the insect maps after the ELC emphasizes that the ELC of the crystal structure is veering off the straight path of the IFM envelope toward the bend of the chicken RLC.

Table 1

Image Processing Results

Myosin Isoform	Data Sets*	Average Phase Residual	# of 1140 Å Actin Repeats
CSk	37	29.7 (21.5–38.2)**	150
Leth	56	25.3 (18.1–29.9)**	185
wt Dros	40	33.8 (23–47)**	76
IFI-EC	29	39.2 (32–44.2)**	81

* Denotes the number of near and far side data sets in average.

** Numbers in parenthesis denote the minimum and maximum phase residual.